Available online at www.sciencedirect.com
ScienceDirect
European Journal of Mechanics B/Fluids 25 (2006) 565–573

Nonlinear wave amplification in front of reflective structures

E. Jamois [a,b], B. Molin [a,*], F. Remy [a], O. Kimmoun [a]

[a] *École Généraliste d'Ingénieurs de Marseille, 13 451 Marseille cedex 20, France*
[b] *Saipem SA, 78 884 Saint-Quentin Yvelines cedex, France*

Received 20 October 2005; received in revised form 9 January 2006; accepted 10 January 2006

Available online 5 June 2006

Abstract

For the design of marine and coastal structures subject to nonlinear waves in deep to shallow water, it is crucial to take into account both wave/structure and wave/wave interactions. A critical phenomenon involving large wave amplifications on the weather side of reflective structures has been recently observed during experimental campaigns. It appears for a wide range of wavelengths, when compared to the size of the structure, and it is directly related to third order interactions in the wave steepness. This induces high free surface elevations, known as 'run-ups', associated with high local loads that can damage the structure. In this paper, we pursue theoretical and numerical calculations using two approaches: a steady-state spectral solution and time-domain simulations using a high-order Boussinesq model. Cases involving normal and oblique wave interaction with a vertical rigid plate are investigated.

Keywords: Wave–structure interactions; Nonlinear waves; Oblique waves; Spectral solution; Boussinesq model

1. Introduction

This paper focuses on a large wave amplification phenomenon occurring in front of reflective marine or coastal structures and due to tertiary interactions between the incoming and the reflected wave fields. These nonlinear wave interactions take place over a wide area on the weather side of the structure. Several experiments involving a rectangular barge model and different bottom-mounted structures in deep and shallow water were carried out on this topic. A striking feature of these tests was large amplifications of waves on the weather-side of the structure, that depended both upon the wavelengths and the steepnesses of the incoming waves. A physical interpretation of the phenomenon was proposed by Molin et al. [1]: it advocates that the reflected wave fields tend to slow down the incoming waves by reducing their wavelengths due to third order interactions in the wave steepness, thus acting as a shoal. As a consequence, the incoming crest-lines bend and the wave energy gets focused toward the center of the structure.

We extend here the theoretical model proposed by Molin et al. [1] to oblique incoming waves and compare it to numerical simulations using the Boussinesq-type model presented in Jamois et al. [2,3]. Results obtained on a vertical plate, submitted to both normal and oblique regular waves, are presented.

* Corresponding author.
E-mail address: bernard.molin@egim-mrs.fr (B. Molin).

0997-7546/$ – see front matter
doi:10.1016/j.euromechflu.2006.01.004

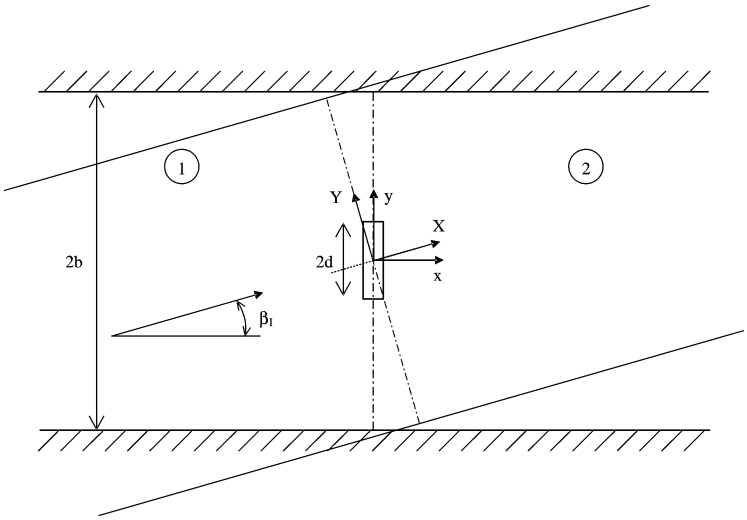

Fig. 1. Theoretical fluid domain geometry.

2. Theoretical model

We propose here a theoretical model, based on a frequency domain approach, and accounting for tertiary wave interactions. The theoretical wave tank, depicted in Fig. 1, is divided into two sub-domains on either side of the plate, bounded by the basin walls located at $y = \pm b$. The vertical surface piercing rigid plate, of zero thickness and width $2d$, is located at the center of the tank. For the sake of simplicity, the depth is supposed to be infinite. The plate is submitted to regular incident waves that propagate obliquely along the β_I-direction.

2.1. Resolution of the linearized diffraction problem

For the particular fluid domain geometry considered here, the linearized diffraction problem can be solved semi-analytically in the frequency domain. Considering the irrotational flow of an incompressible inviscid fluid with a free surface, a cartesian coordinate system is adopted, with the x- and y-axis located in the still-water plane $z = 0$ and with the z-axis pointing vertically upwards. We look for a steady-state solution of the form:

$$\phi(x, y, z, t) = \mathcal{R}e\left\{\varphi(x, y, z)\mathrm{e}^{-\mathrm{i}\omega t}\right\}. \tag{1}$$

In the left-hand side sub-domain ($x \leqslant 0$), the velocity potential φ can be expressed as:

$$\varphi_1 = \frac{-\mathrm{i}A_I g}{\omega}\mathrm{e}^{kz}\left\{\mathrm{e}^{\mathrm{i}(kx\cos\beta_I + ky\sin\beta_I)} + \sum_{n=0}^{\infty} B_n \mathrm{e}^{-\mathrm{i}\alpha_n x}\cos\lambda_n(y+b)\right\}, \tag{2}$$

and, in the right-hand side sub-domain ($x \geqslant 0$) as:

$$\varphi_2 = \frac{-\mathrm{i}A_I g}{\omega}\mathrm{e}^{kz}\left\{\mathrm{e}^{\mathrm{i}(kx\cos\beta_I + ky\sin\beta_I)} + \sum_{n=0}^{\infty} C_n \mathrm{e}^{\mathrm{i}\alpha_n x}\cos\lambda_n(y+b)\right\}, \tag{3}$$

where A_I, ω, k and β_I are respectively the amplitude, the angular frequency, the wave number and the direction of the incident wave field. In these expressions, $\lambda_n = n\pi/(2b)$. For $n \leqslant N$, where N is the largest integer n such that λ_n is smaller than k, the modes are progressive; for $n > N$, they are evanescent. Consequently, $\alpha_n = \sqrt{k^2 - \lambda_n^2}$ for $n \in [0,\ N]$ and $\alpha_n = \mathrm{i}\sqrt{\lambda_n^2 - k^2}$ for $n \in [N+1,\ \infty[$.

Eqs. (2) and (3) express that the diffracted wave system reflects on the side-walls at $y = \pm b$ while the incoming waves propagate freely through the walls! This is not physical but, as long as the walls are taken sufficiently far away, the combined wave-field in the vicinity of the plate is the same as in an unbounded ocean. Confinements effects are present in physical wave-tanks as well, with both the incoming and diffracted wave-systems being reflected by the walls.

Matching of the x-velocity components φ_{1x} and φ_{2x} on the common boundary $x = 0$ for $y \in [-b,\ b]$ yields that $C_n = -B_n$.

Then, setting the no-flow condition $\varphi_{1x} = 0$ for $y \in [-d,\ d]$ and matching φ_1 and φ_2 for $y \in [-b,\ -d] \cup [d,\ b]$, gives:

$$B_m b(1+\delta_{m0}) + \sum_{n\neq m} B_n \left(\frac{\alpha_n}{\alpha_m} - 1\right) \int_{-d}^{d} \cos\lambda_m(y+b)\cos\lambda_n(y+b)\,\mathrm{d}y$$

$$= \frac{k\sin\beta_I}{\alpha_m} \int_{-d}^{d} \mathrm{e}^{\mathrm{i}ky\sin\beta_I} \cos\lambda_m(y+b)\,\mathrm{d}y. \tag{4}$$

This linear system is solved with a standard Gauss algorithm.

It has been checked that the obtained elevations along the weather side of the plate are in agreement with the results presented in Goda [4] (Fig. 3.44).

2.2. Accounting for tertiary interactions

We introduce another frame of reference OXY where OX corresponds to the incoming wave propagation direction β_I (see Fig. 1). Following Molin et al. [1], we express the incoming wave potential φ_I as:

$$\varphi_I(X,Y,z) = \frac{-\mathrm{i}A(\epsilon^2 X, \epsilon Y)g}{\omega} \mathrm{e}^{(k+\epsilon^2 k^{(2)}(\epsilon^2 X,\epsilon Y))z} \mathrm{e}^{\mathrm{i}k(1-\epsilon^2)X}. \tag{5}$$

The Laplace equation, to the order $\epsilon^2 \equiv k^2 A_I^2$, yields

$$2\mathrm{i}kA_X + A_{YY} + 2k^4 A_I^2 A + 2kk^{(2)}A = 0. \tag{6}$$

The modification $k^{(2)}$ of the wave number k is obtained from

$$k^{(2)} = k^3 A_R^2 f(\beta_R - \beta_I) - k^3 A A^*, \tag{7}$$

with the interaction function $f(\beta)$ given by Eq. (3.4) in Molin et al. [1].

Here A_R and β_R are, respectively, the (real) amplitude and direction of the plane wave locally equivalent to the reflected wave-field by the plate.

Finally the following parabolic equation is obtained that describes the spatial evolution of $A(X,Y)$ under tertiary interaction with the reflected wave system:

$$2\mathrm{i}kA_X + A_{YY} + 2k^4\left[A_R^2 f(\beta_R - \beta_I) + A_I^2 - AA^*\right]A = 0. \tag{8}$$

New fictitious walls located at $Y = \pm b$ are introduced and, taking advantage of this confined geometry, $A(X,Y)$ is expanded under the form:

$$A(X,Y) = A_I\left(1 + \sum_{n=0}^{\infty} a_n(X)\cos\lambda_n(Y+b)\right), \quad \lambda_n = \frac{n\pi}{2b}. \tag{9}$$

The resulting set of equations in $a_n(X)$ is integrated in X, starting from some distance l (where it is assumed that $a_n(-l) \equiv 0$) all the way to the plate. In the applications presented below the distance l has been taken equal to 16 wavelengths.

2.3. New resolution of the diffraction problem

The diffraction problem is then solved again with the modified incoming wave field due to the tertiary interactions occurring in front of the plate. In the left-hand side sub-domain close to the plate, the velocity potential is now written:

$$\varphi_1 = \frac{-\mathrm{i}A_I g}{\omega}\mathrm{e}^{kz}\left\{\left[1+\sum_n a_n(0)\cos\lambda_n(y\cos\beta_I+b)\right]\mathrm{e}^{\mathrm{i}(kx\cos\beta_I+ky\sin\beta_I)} + \sum_{n=0}^{\infty} B_n \mathrm{e}^{-\mathrm{i}\alpha_n x}\cos\lambda_n(y+b)\right\}. \tag{10}$$

The incident and diffracted velocity potentials are thus updated and this process is pursued until convergence is reached, as in Molin et al. [1].

3. Numerical wavetank

For the numerical simulations, we use the Boussinesq-type model described in Jamois et al. [3]. Based on the formulation derived by Madsen et al. [5] (see also Fuhrman and Bingham [6]), the equations are reformulated in terms of a velocity potential. The resulting model is limited to dimensionless water depths of $kh \leqslant 10$ in terms of dispersion, is correctly accounting for nonlinear effects up to $kh \approx 8$, while the complete internal wave kinematics are restricted to $kh \leqslant 4$. Thus the method remains valid for depths that can be considered as infinite. By reducing the number of unknowns within the fluid problem, the use of a velocity potential leads to increased computational efficiency as compared with other approaches based on horizontal velocities. Furthermore, it reveals to be convenient in situations where rectangular box-shaped structures are present in the fluid domain. We take benefit of these numerical advantages to study wave–structure interactions in large domains.

This formulation has been already validated in Jamois et al. [3] on several physical experiments involving highly nonlinear wave/structure interaction in deep water. We use here the extension of the model to oblique wave generation proposed in Jamois et al. [3].

4. Results and comparisons

The wave tank used for the comparisons is 16 m wide, with a length from the wavemakers to the structure of 19 m. This is based on the previous experimental campaigns that were conducted on this topic. The size of the interaction zone between the incident and reflected wave fields guarantees that the run-up phenomenon will be fully developed after a certain time. A vertical rigid plate 2.4 m wide is set up in the middle of the numerical basin. We consider here the wave period $T = 0.88$ s, which for small amplitude waves corresponds to a wavelength $L = 1.2$ m. In this critical case, the wavelength of the incoming wave field corresponds to half the length of the structure thus magnifying the run-ups on the weather-side of the plate. Similar case was considered by Fuhrman et al. [7], albeit at a smaller steepness (4%).

Nonlinear regular waves of steepness equal to $H/L = 2\eta_0/L = 5\%$ are generated for three different incidences, 0°, 10° and 20°. In the computations of the spectral solution, the series expansions (2) and (3) have been truncated to include up to 200 terms. In the Boussinesq model, the discretizations used are $\Delta x = \Delta y = 0.061$ m $\approx L/20$ (to optimize the length and the location of the plate), and $\Delta t = T/20 = 0.044$ s. The plate dimensions are $2\Delta x \times 2.38$ m; $2\Delta x$ corresponds to the minimum achievable thickness for any structure due to the 5×5 square stencil used in space. To stay within the optimal range of the model while still solving a deep water problem, the depth is set to $h = 0.78$ m, i.e. $kh \approx 4$. As a reference, for normal incidence, a simulation for 1700 time steps (≈ 75 s) over a computational domain of total size 263×434 grid points, requires 6.5 hours (on a single Pentium 4 2.8 GHz processor with 1024 MB DDR-RAM).

Fig. 2 shows the numerical and experimental time series of the free surface elevation, normalized by the incident wave field amplitude, at the middle of the plate on the weather-side and for the case of normal incidence. The experimental time series is taken from the model tests reported in Molin et al. [1]. It can be seen that the two time series are in good agreement, with similar transients that last over about 25 cycles. Over the steady state part, waves of heights more than five times larger than the incoming waves are obtained. Within the stationary state, a period tripling effect as previously reported by Jiang et al. [8] and Longuet-Higgins and Drazen [9] develops.

To further demonstrate the extreme nonlinearity involved within this simulation, we present the computed envelope from the wavemaker to the plate along the centerline $y = 0$ in Fig. 3 (note that in this figure the origin of the coordinate system is shifted to the left of the wave generation zone, about 20 m ahead of the plate). This is extracted from the simulation after the steady-state has been reached.

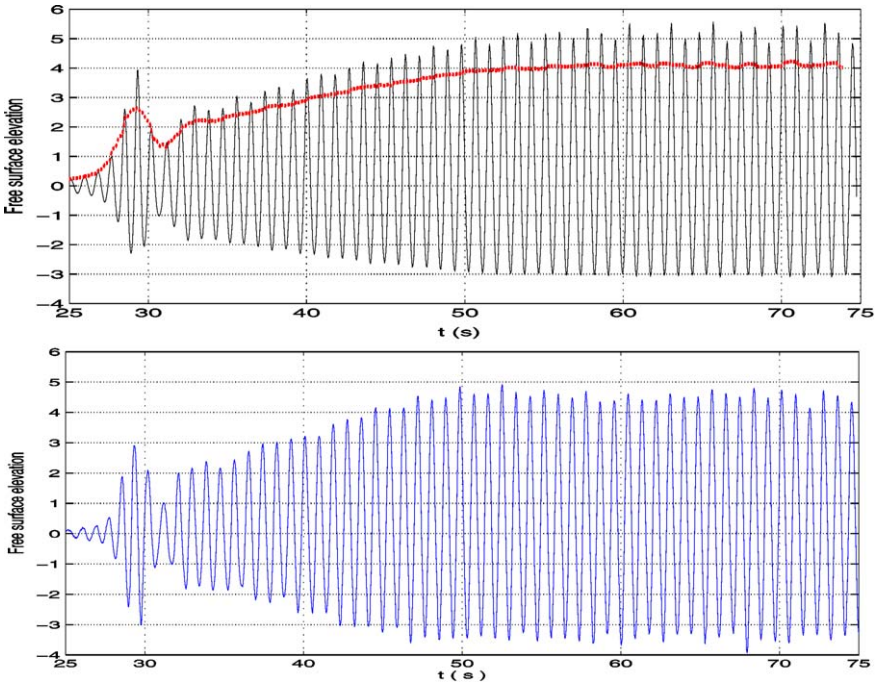

Fig. 2. Numerical (top) and experimental (bottom) time series of the free surface elevation at the middle of the plate on the weather side for the case of normal incidence. The dashed line shows the time evolution of the RAO (Response Amplitude Operator).

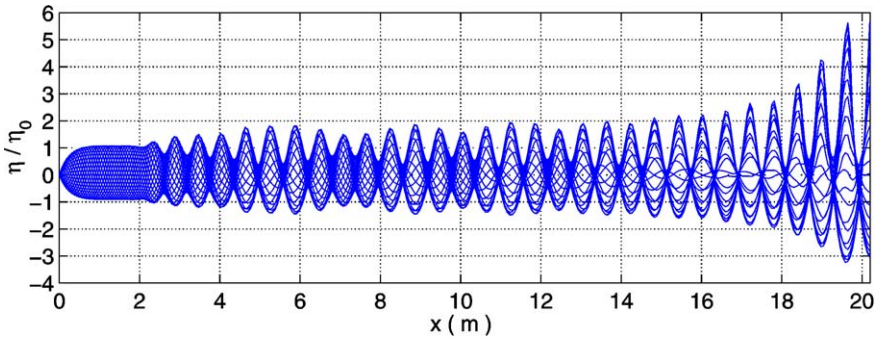

Fig. 3. Computed free surface profiles along the centerline for normal incidence, $T = 0.88$ s and $H = 0.062$ m.

To gain insight into the physical mechanism of the run-up phenomenon occurring here, four snapshots corresponding to different instants over half a wave period, once a stationary state has developed over the domain, are given in Fig. 4. As a result of reflections from the plate, highly nonlinear standing waves take place on its weather side, with the highest wave located half a wavelength away, as depicted in snapshot (a) (see also Fig. 3). This figure clearly shows a noticeable curvature of the crest lines over a couple of wavelengths, confirming the contention of Molin et al. [1]. This curvature induces wave focusing toward the middle of the plate.

At time t_0, the wave crest by the edge of the picture, marked with an arrow, is about to impact the plate. At time $t_0 + T/5$, the plate is impacted at both sides and waves arising from these two points then propagate toward the middle of the plate, where their gathering creates a large wave amplification at time $t_0 + T/2$.

The steady-state Response Amplitude Operator (RAO) of the computed free surface profile along the weather side of the plate, is given in Fig. 5 for normal incidence. This has been obtained by Fourier analysis over a sliding window, two periods long. The results of both approaches are compared. As a reference, linear theory predictions are also given.

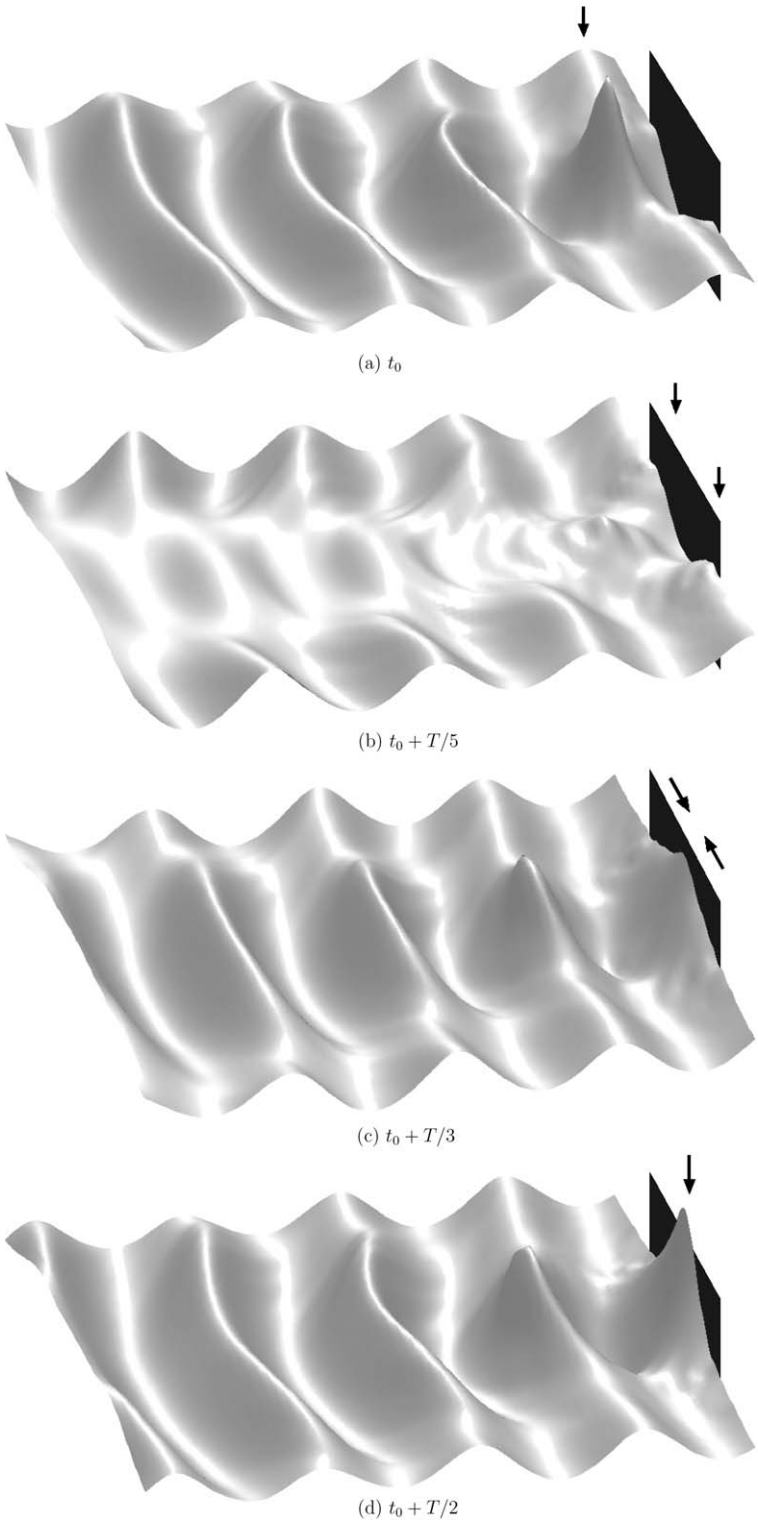

Fig. 4. Run-up phenomenon mechanism in normal incidence.

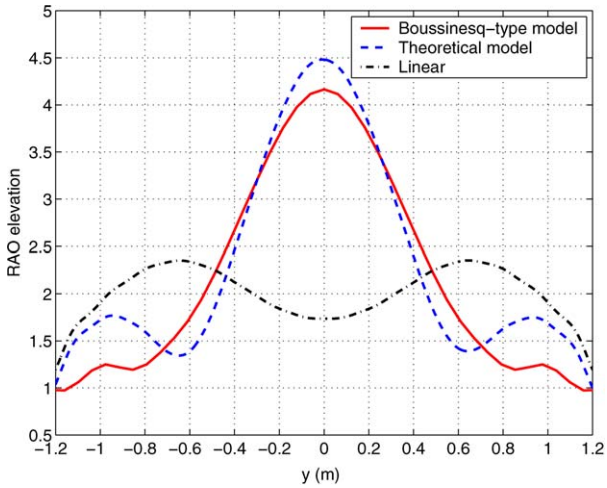

Fig. 5. Comparison of the computed free surface RAOs along the weather-side of the plate for normal incidence and $H/L = 5\%$.

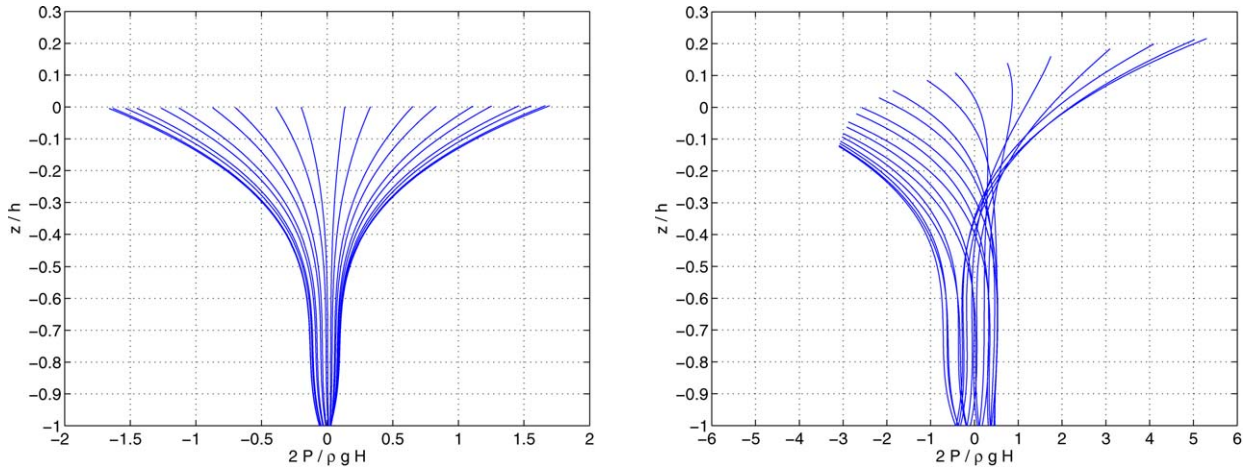

Fig. 6. Vertical pressure profiles along the middle of the weather side of the plate, for normal incidence. (a) Steepness 0.3%. (b) Steepness 5%.

We observe that the semi-analytical model predicts a larger run-up amplitude than the Boussinesq formulation. This discrepancy may be due to the restrictive theoretical assumptions inherent to the semi-analytical model: the complex amplitude A of the incoming waves is assumed to vary slowly in space (see Eq. (5)); the reflected wave-system is locally idealized by a plane wave; nonlinear effects higher than third-order are not accounted for. Another noticeable difference lies with the second local maxima, by the edges of the plate, predicted by the theoretical model: they are hardly visible in the Boussinesq computation.

These high free surface elevations lead to important pressure loads on the structure. Fig. 6 shows the vertical pressure profiles, computed by the Boussinesq model using the Bernoulli equation (the hydrostatic component being excluded), along the middle of the plate for normal incidence. Firstly, the Boussinesq-type model was run with a wave steepness H/L equal to 0.3%. At such a low steepness, nonlinear effects hardly appear. In these conditions, as it can be seen in Fig. 6(a), the vertical pressure profiles are of the shape predicted by Stokes linear theory and perfectly symmetric. Under incoming waves of steepness 5%, the vertical pressure profiles are affected by non-linearities and they become strongly asymmetric. The different curves are crossing each other, reflecting the fact that, down the water column, the dominant frequency in the time series of the vertical pressure is 2ω: in the deep water case considered here, the first order component decays quickly through the water column down to the sea-bed, while the second-order bound harmonic component remains nearly constant.

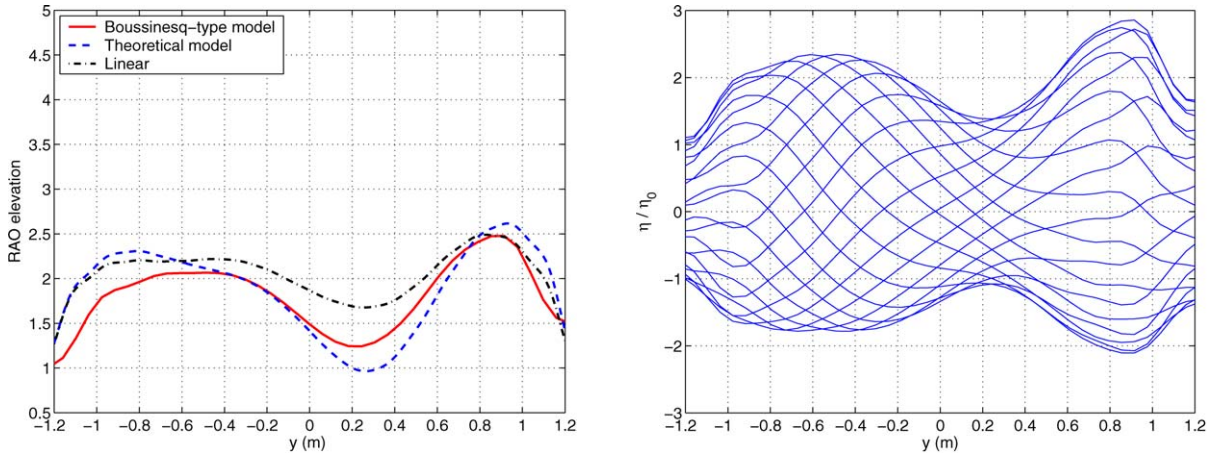

(a) (b)

Fig. 7. (a) Comparison of the computed free surface RAOs along the weather-side of the plate for $\beta_I = 10°$ and $H/L = 5\%$. (b) Fully nonlinear steady-state free surface envelope along the weather-side of the plate computed by the Boussinesq-type approach.

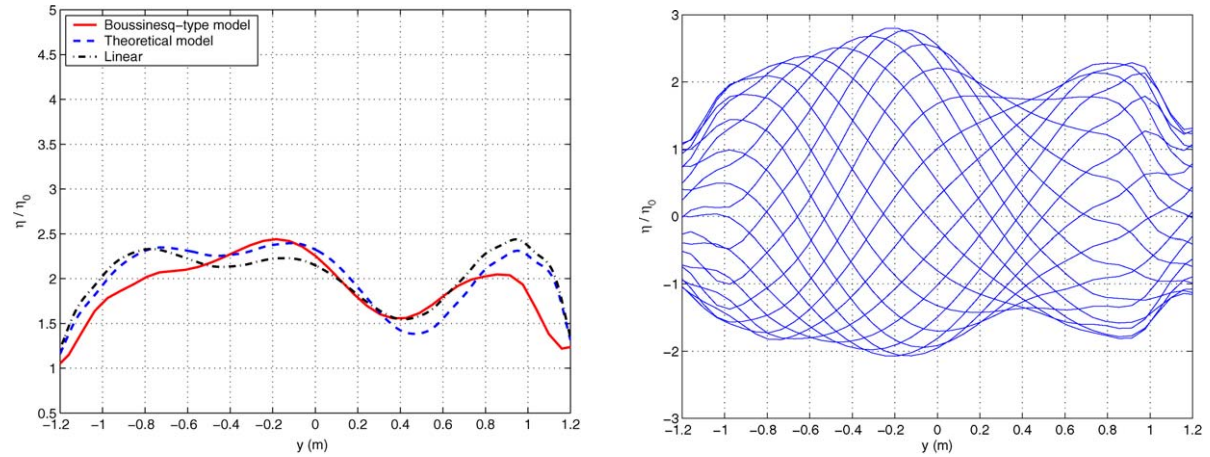

(a) (b)

Fig. 8. (a) Comparison of the computed free surface RAOs along the weather-side of the plate for $\beta_I = 20°$ and $H/L = 5\%$. (b) Fully nonlinear steady-state free surface envelope along the weather-side of the plate computed by the Boussinesq-type approach.

For an angle of incidence of 10° (cf. Fig. 7), the results get closer to the linear theory. A fair agreement between both models is obtained. The main effect of the nonlinearity is here to increase the trough in the RAO curve by the middle of the plate. In Fig. 7(b), the fully nonlinear free surface envelope along the weather side of the plate after a steady-state has been achieved, is given. The maximum factor of amplification is nearly 3 thus still slightly higher than a classical linear result.

Finally, Fig. 8 presents the results obtained for an incidence of 20°. It can be seen that both nonlinear models give results that are very close to linear theory. The maximum of the free surface envelope is now located on the upwave side of the plate, contrary to the incidence $\beta_I = 10°$. It should be noted that for this case the steady state is immediately reached in the numerical simulation, further highlighting a behavior close to a linear case.

5. Concluding remarks

The numerical results shown here support the contention of Molin et al. [1] that the run-up effect is due to nonlinear interactions between the incoming and reflected wave-fields: as the incidence angle deviates from normal direction,

the strength of the reflected wave-system, traveling in the opposite direction to the incoming waves, gets smaller, and the interaction area also decreases in size. As a result the incoming waves are much less affected than in the perpendicular case.

In this paper we have focused on free surface elevations along the plate. However it is clear from Fig. 3 that these high elevations are also observed away from the plate. It might therefore be questioned whether such energy concentration effects could be met some distance from an irregularly reflective coastline. In this respect the run-up effect studied here could have some relevance to the rogue wave phenomenon.

References

[1] B. Molin, F. Remy, O. Kimmoun, E. Jamois, The role of tertiary wave interactions in wave-body problems, J. Fluid Mech. 528 (2005) 323–354.
[2] E. Jamois, O. Kimmoun, B. Molin, Y. Stassen, Nonlinear interactions and wave run-up near a gravity base structure, in: Proc. 29th ICCE Conf., vol. 4, Lisbon, 2004, pp. 3979–3991.
[3] E. Jamois, D.R. Fuhrman, H.B. Bingham, B. Molin, A numerical study of nonlinear wave run-up on a vertical plate, Coastal Engineering (2005), in press.
[4] Y. Goda, Random Seas and Design of Maritime Structures, University of Tokyo Press, 1985.
[5] P.A. Madsen, H.B. Bingham, H.A. Schäffer, Boussinesq-type formulations for fully nonlinear and extremely dispersive water waves, Proc. Roy. Soc. London A 459 (2003) 1074–1104.
[6] D.R. Fuhrman, H.B. Bingham, Numerical solutions of fully non-linear and highly dispersive Boussinesq equations in two horizontal dimensions, Int. J. Numer. Methods Fluids 44 (2004) 231–255.
[7] D.R. Fuhrman, H.B. Bingham, P.A. Madsen, Nonlinear wave–structure interactions with a high-order Boussinesq model, Coastal Engrg. 52 (2005) 655–672.
[8] L. Jiang, M. Perlin, W.W Schultz, Period tripling and energy dissipation of breaking standing waves, J. Fluid Mech. 369 (1998) 273–299.
[9] M.S. Longuet-Higgins, D.A. Drazen, On steep gravity waves meeting a vertical wall: a triple instability, J. Fluid Mech. 466 (2002) 305–318.